

Orbital Control of Long-Range Transport in Conjugated and Metal-Centered Molecular Electronic Junctions

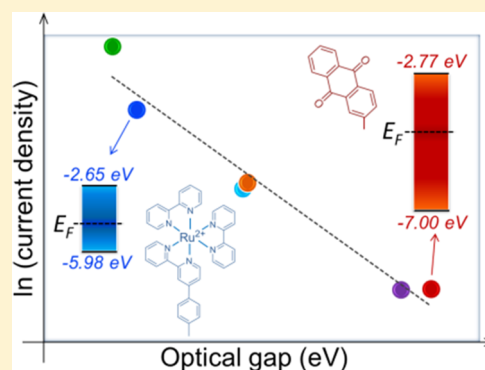
Ushula M. Tefashe,[†] Quyen Van Nguyen,^{‡,ib} Amin Morteza Najarian,^{†,ib} Frederic Lafolet,^{‡,ib} Jean-Christophe Lacroix,^{*,‡,ib} and Richard L. McCreery^{*,†,ib}

[†]Department of Chemistry, University of Alberta, 11421 Saskatchewan Drive, Edmonton, Alberta T6G 2M9, Canada

[‡]Université Paris Diderot, Sorbonne Paris Cité, ITODYS, UMR 7086 CNRS, 15 rue Jean-Antoine de Baïf, 75205 Paris Cedex 13, France

S Supporting Information

ABSTRACT: Large area molecular junctions consisting of covalently bonded molecular layers between conducting carbon electrodes were compared for Co and Ru complexes as well as nitroazobenzene and anthraquinone to investigate the effect of molecular structures and orbital energies on electronic behavior. A wide range of molecular layer thickness (d) from 1.5–28 nm was examined and three distinct transport regimes in attenuation plots of current density (J) vs thickness were revealed. For $d < 5$ nm, the four molecular structures had comparable current densities and thickness dependence despite significant differences in orbital energies, consistent with coherent tunneling and strong electronic coupling between the molecules and contacts. For $d > 12$ nm, transport depends on the electric field rather than bias, with the slope of $\ln J$ vs d near-zero when plotted at a constant electric field. At low temperature ($T < 150$ K), transport is nearly activationless and likely occurs by sequential tunneling and/or field-induced ionization. For $d = 5$ –10 nm, transport correlates with the energy gap between the highest occupied and lowest unoccupied molecular orbitals, and $\ln J$ is linear with the square root of the bias or electric field. Such linearity occurs for all three transport regimes and is consistent with the energy barrier lowering by the applied electric field. The results clearly indicate a strong dependence of charge transport on molecular orbital energies provided $d > 5$ nm, with a variation of 7 orders of magnitude of J for different molecules and $d = 10$ nm. The results provide insights into charge transport mechanisms as well as a basis for rational design of molecular electronic devices.



INTRODUCTION

A long-standing and fundamental question in the field of molecular electronics is the relationship between the molecular structure and electronic behavior of “molecular junctions (MJs)” consisting of single molecules or ensembles of many molecules oriented between two conducting contacts. When the transport distance, d , is in the range of 1–30 nm between the contacts, the charge transport mechanism may differ fundamentally from those in “organic electronic” devices, where d usually exceeds 50 nm.^{1–4} The rational design of molecular devices with useful electronic behavior should depend on molecular structures, and presumably on the molecular orbital energies and their interactions with the contacts and/or adjacent molecules. Coherent quantum mechanical tunneling is generally accepted as the dominant mode of transport when $d < 2$ nm for aliphatic molecules and $d < 5$ nm for conjugated systems, with the tunneling barrier determined by the energy of occupied or unoccupied molecular orbitals relative to the electrode Fermi level. However, strong electronic coupling between aromatic molecules and conducting contacts can diminish the effects of orbital energies, leading to minor effects on transport from

>2 eV variation in highest occupied molecular orbital (HOMO) or lowest unoccupied molecular orbital (LUMO) energy when $d < 5$ nm.^{5,6} The exponential dependence of tunneling on d is often manifested by linear plots of $\ln J$ vs d , where J is the current density at a given bias, with a slope equaling the attenuation coefficient β with units of nm^{-1} . Many investigators have reported $\beta = 2$ – 3 nm^{-1} for π -conjugated structures across different junction designs (e.g., single molecule and large area MJs) as well as departures from linearity of $\ln J$ vs d attributed to a change in the mechanism to various incoherent, “hopping” mechanisms^{7–9} or to resonant tunneling.^{10,11} Several examples of major departures from the 2 – 3 nm^{-1} range include porphyrins ($\beta < 0.06 \text{ nm}^{-1}$),^{10,11} organometallics ($\beta < 0.03 \text{ nm}^{-1}$),^{12,13} and viologen oligomers.^{14,15} Molecular junctions containing metal centers have been shown to conduct over large distances exceeding 40 nm, with the possible involvement of redox reactions underlying transport.^{11–13}

Received: October 12, 2018

Revised: November 26, 2018

Published: November 28, 2018

Scheme 1

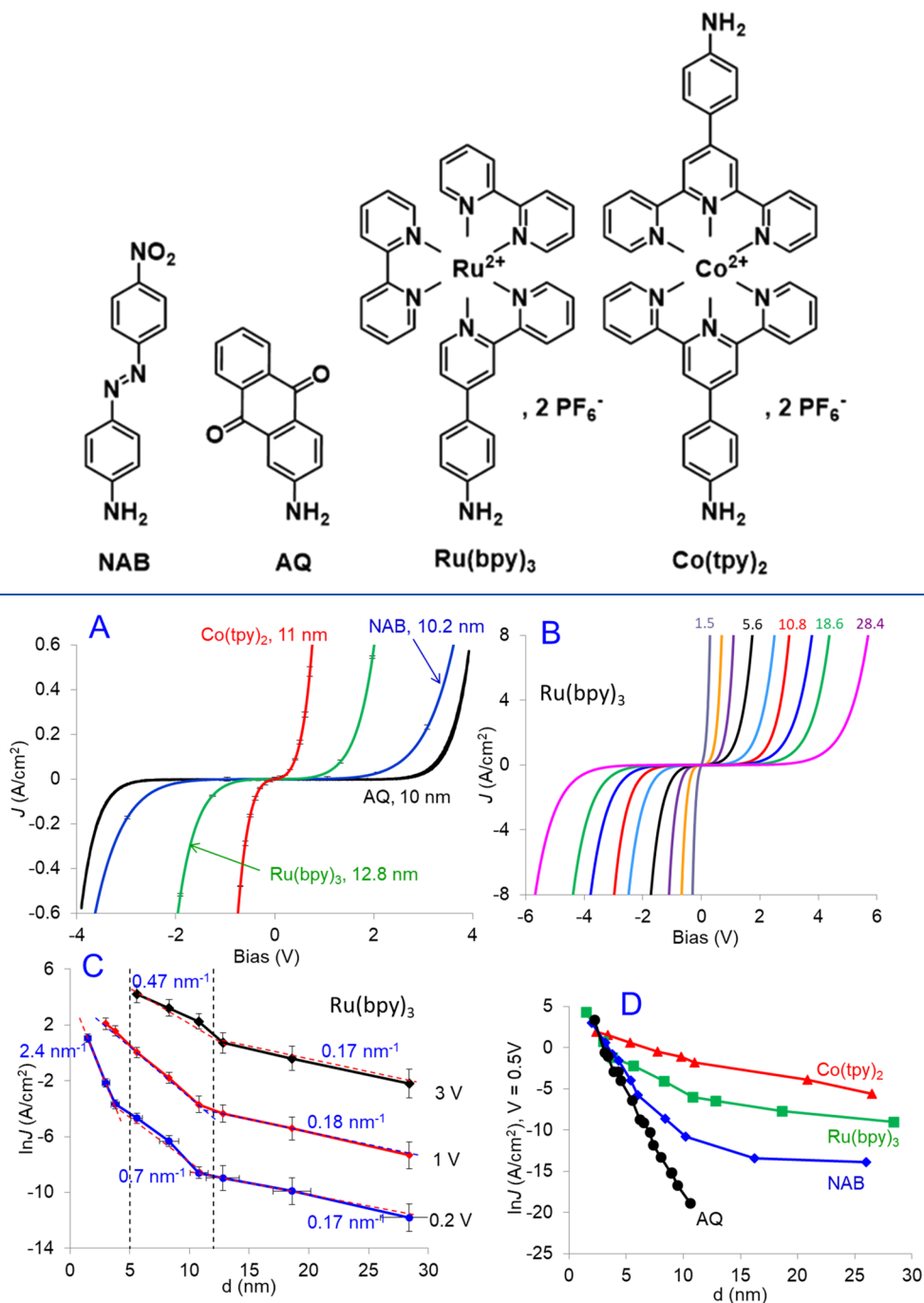


Figure 1. (A) *JV* responses for Co(tpy)₂, Ru(bpy)₃, NAB, and AQ MJs with a similar thickness of 10–13 nm. (B) *JV* curves for different thicknesses of Au₃₀/eC₁₀/Ru(bpy)₃/eC₃/Au₂₀ MJs with the numbers on each curve denoting Ru(bpy)₃ layer thickness in nm. (C) Attenuation plots for Ru(bpy)₃ junctions for the bias values indicated to the right of each curve and slopes (β) indicated. (D) Attenuation plots for Co(tpy)₂, Ru(bpy)₃, NAB, and AQ devices obtained at 0.5 V bias. Error bars in (A) and (C) represent \pm standard deviation for four or more junctions.

The current investigation was motivated in part to understand transport beyond the coherent tunneling range of ~ 5 nm for π -conjugated MJs, with particular interest in the role of structures and orbital energies in controlling transport. The amine precursors of the four molecules studied are shown in Scheme 1, and MJ fabrication is described in Supporting Information (SI) Sections 1–5.

We reported previously that aromatic molecules with a HOMO–LUMO (H–L) gap less than ~ 4 eV showed a

significant departure from linearity of plots once d exceeded 4 nm, and proposed transport by sequential tunneling,⁶ possibly preceded by field-induced ionization.^{16,17} In addition, departure from a $\beta = 2.4$ nm⁻¹ line was observed for both nitroazobenzene (NAB) and a Ru(bpy)₃ derivative, with light emission from Ru(bpy)₃ indicating that both the HOMO and LUMO orbitals were involved in transport.¹⁸ Earlier work with bis-thienyl benzene (BTB) junctions revealed three regions of linearity in β plots, with significant field-dependent current

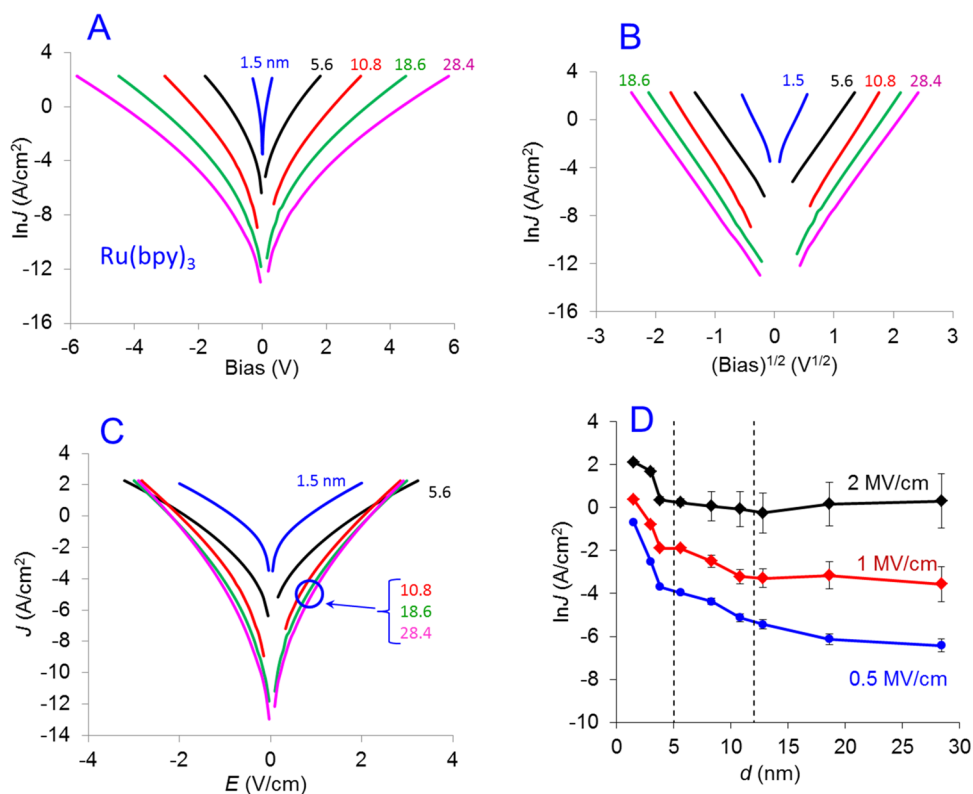


Figure 2. (A) JV curves in semilogarithmic scale for different thicknesses of Ru(bpy)₃. (B) $\ln J$ vs $V^{1/2}$ for the same series of Ru(bpy)₃ junctions shown in (A). (C) $\ln J$ vs E plots for different thicknesses of Ru(bpy)₃. (D) Attenuation plots for Ru(bpy)₃ MJs at a constant field, $E = 0.5, 1.0,$ and 2 MV/cm. Additional thicknesses are provided in SI Figure S4.

density even at low temperature (<10 K).¹⁶ Using the same carbon/molecule/carbon junction design for all molecules, we extended these comparisons to include a cobalt terpyridyl derivative and a broader range of thickness and temperature, with the primary goal of relating transport to orbital energies. In particular, we sought to investigate the possibility of orbital transport, in which carriers enter orbitals by redox events with or without reorganization.

RESULTS

Current density vs bias voltage (JV) curves for Ru(bpy)₃, Co(tpy)₂, NAB, and anthraquinone (AQ) molecular junctions with electron-beam deposited carbon (eC) contacts¹⁹ and similar molecular layer thicknesses in the range of $d = 10$ – 12 nm are shown in Figure 1A, all obtained in a vacuum at a scan rate of 1000 V/s (molecular structures and fabrication details are provided in Supporting Information (SI) Sections 1–5). The curves are averages of at least four MJs with typical error bars shown in each case, and are stable for hundreds of JV scans. The JV responses of all four examples are symmetric with respect to polarity, and the lack of rectification is not surprising given the compositional symmetry of eC/molecule/eC MJs. The variation in J by orders of magnitude over the four molecules clearly indicates a strong dependence on the molecular structure and the additional results described here were directed toward understanding its origin. JV curves for the Ru(bpy)₃ case are shown for a wide range of thickness ($d = 1.5$ – 28.4 nm) in Figure 1B.

Although the symmetry and shape of the responses are maintained over this range, there are distinct regions for the dependence of J on thickness, apparent in Figure 1C. As noted

previously,¹⁸ Ru(bpy)₃ exhibits two linear regions for $V = 0.2$ V and $d < 12$ nm, with $\beta = 2.4$ nm⁻¹ for $d < 4$ nm and $\beta = 0.7$ nm⁻¹ for $d = 4$ – 10 nm. These two regions persist for high bias up to 3 V, albeit with a gradual decrease in slope for the 4– 10 nm range. A third linear region is apparent for $d = 12$ – 28.4 nm, with β constant at ~ 0.18 nm⁻¹ for the bias range of 0.2–3 V. JV curves for a similarly wide range of thickness for NAB and Co(tpy)₂ in the same MJ structure are shown in SI Figure S5 and are compared to AQ reported previously⁶ in the attenuation plot of Figure 1D. Note that all four MJ types have similar current density for $d < 4$ nm, which we attribute to strong electronic coupling discussed in detail previously.⁵ As d increases above ~ 5 nm, the attenuation plots diverge rapidly, consistent with their very different JV response for $d \approx 10$ nm (Figure 1A). Note that $J(0.5$ V) for Co(tpy)₂ exceeds that of AQ by a factor of $>10^7$ when $d = 10$ nm.

To further investigate the changes in attenuation slopes apparent in Figure 1C,D, the Ru(bpy)₃ results were examined in greater detail. Figure 2A shows the entire range of thicknesses studied, plotted as $\ln J$ vs V . All cases show nonlinear behavior, whereas the same data plotted as $\ln J$ vs $V^{1/2}$ (Figure 2B) is linear with correlation coefficients (R^2) > 0.998 across the entire thickness range. The slopes for positive bias decreased with thickness from 10.8 V^{-1/2} for $d = 1.5$ and 3.8 nm to ~ 7 V^{-1/2} for $d = 12.8$ nm. This unexpected linearity of $\ln J$ vs $V^{1/2}$ was reported previously for fluorene (FL) and anthraquinone using the same MJ structure as the current results⁶ and for BTB.^{6,16} Several classical transport mechanisms such as Schottky emission and Poole–Frenkel transport are dependent on the electric field rather than applied bias, and we reported previously that transport in BTB layers with $d > 8$ nm

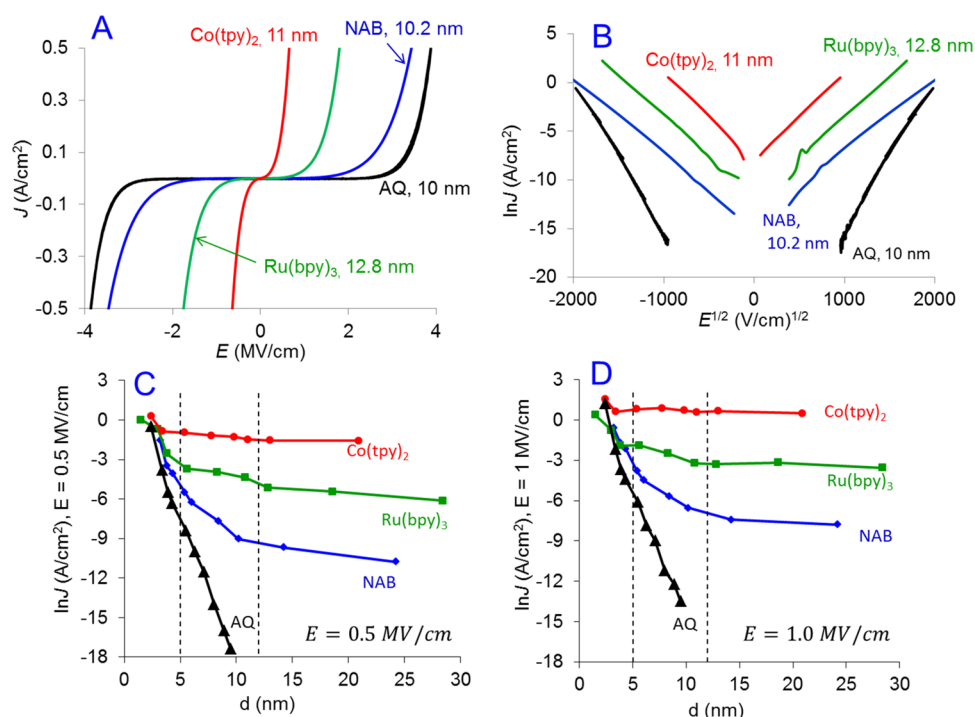


Figure 3. (A) Comparison of JE curves $\text{Co}(\text{tpy})_2$, $\text{Ru}(\text{bpy})_3$, NAB, and AQ with a similar thickness of 10–13 nm, shown in panel Figure 1A. (B) $\ln J$ vs $E^{1/2}$ plots of the curves shown in panel (A). (C) Attenuation plots for the four molecules plotted at a constant field (C) 0.5 MV/cm and (D) 1 MV/cm.

Table 1. β (nm^{-1}) for the Three Regions in the Attenuation Plot at Constant V and E

constant V	0.5 V				1.0 V			
	$\text{Co}(\text{tpy})_2$	$\text{Ru}(\text{bpy})_3$	NAB	AQ	$\text{Co}(\text{tpy})_2$	$\text{Ru}(\text{bpy})_3$	NAB	AQ
slope 1 (2–5 nm)	0.45	2.37	2.00	3.02	0.35	0.64	2.28	2.46
slope 2 (5–12 nm)	0.39	0.73	1.36	2.52	0.38	0.71	1.18	2.25
slope 3 (12–30 nm)	0.24	0.15	0.18	N/A	0.29	0.21	0.32	N/A
constant E	0.5 MV/cm				1.0 MV/cm			
	$\text{Co}(\text{tpy})_2$	$\text{Ru}(\text{bpy})_3$	NAB	AQ	$\text{Co}(\text{tpy})_2$	$\text{Ru}(\text{bpy})_3$	NAB	AQ
slope 1 (2–5 nm)	1.147	1.291	2.234	2.51	0.950	0.962	1.412	2.27
slope 2 (5–12 nm)	0.077	0.225	0.701	1.67	0.019	0.253	0.545	1.59
slope 3 (12–30 nm)	0.008	0.059	0.121	N/A	0.013	0.020	0.078	N/A

were clearly E -field dependent.¹⁶ For $\text{Ru}(\text{bpy})_3$, Figure 2C shows a plot of $\ln J$ vs electric field (E , MV/cm) for the same curves as in Figure 2A and $d = 1.5$ –28.4 nm. When d exceeds 5 nm, the $\ln J$ vs E curves nearly superimpose over a wide range of current density, implying that transport has become field dependent rather than bias dependent for $d > 10$ nm. Furthermore, plots of $\ln(J/E)$ vs $E^{1/2}$ shown in Figure S4D are linear and overlap for $d > 10$ nm, as was observed previously for BTB, even for $T < 10$ K.¹⁶

The weak dependence of $\ln J$ on thickness is more evident in Figure 2D, which plots $\ln J$ vs d for three values of the applied field. J decreases exponentially for $d < 5$ nm at constant E and continues to decrease with thickness up to $d = 28$ nm. However, $\ln J$ vs d is nearly flat for $d > 12$ nm at higher fields of 1–2 MV/cm, as is consistent for transport controlled by the electric field rather than bias. As indicated by the vertical dashed lines at $d = 5$ and 12 nm, three attenuation regions are not as pronounced at the constant field than at constant V (Figure 1C). Plots of $\ln J$ vs $E^{1/2}$ and $\ln J/E$ vs $E^{1/2}$ yield linear responses for $d = 8$ –28.4 nm (Figure S4D) and nearly overlap

for $d > 10$ nm, similar to previously reported results for BTB junctions with similar device structures.¹⁶

JE plots on a linear scale are compared for AQ, NAB, $\text{Ru}(\text{bpy})_3$, and $\text{Co}(\text{tpy})_2$ in Figure 3A and as $\ln J$ vs $E^{1/2}$ in Figure 3B. As was the case for $\text{Ru}(\text{bpy})_3$, $\ln J$ vs $E^{1/2}$ is linear, although the lower current densities were inaccurate due to sensitivity limitations. As expected from the JV curves of Figure 3A, the magnitudes of $\ln J$ differ significantly for the four molecules and the relationship to the molecular energy levels is discussed below. The attenuation plots made at the constant electric field are shown in Figure 3C,D for $E = 0.5$ and 1.0 MV/cm, and show several interesting effects. First, the three thickness regions observed for NAB and $\text{Ru}(\text{bpy})_3$ at constant bias are maintained and β for both constant V and constant E are listed in Table 1.

Second, for $d < 5$ nm and constant bias, the curves for the four molecules approximately converge, with a slope of 1.5–2.5 nm^{-1} , but significant differences are apparent as d exceeds ~ 4 nm. For either constant V or constant E , the current densities for the four molecules with $d = 10$ nm vary by 7–8 orders of magnitude. Third, a pronounced change to lower

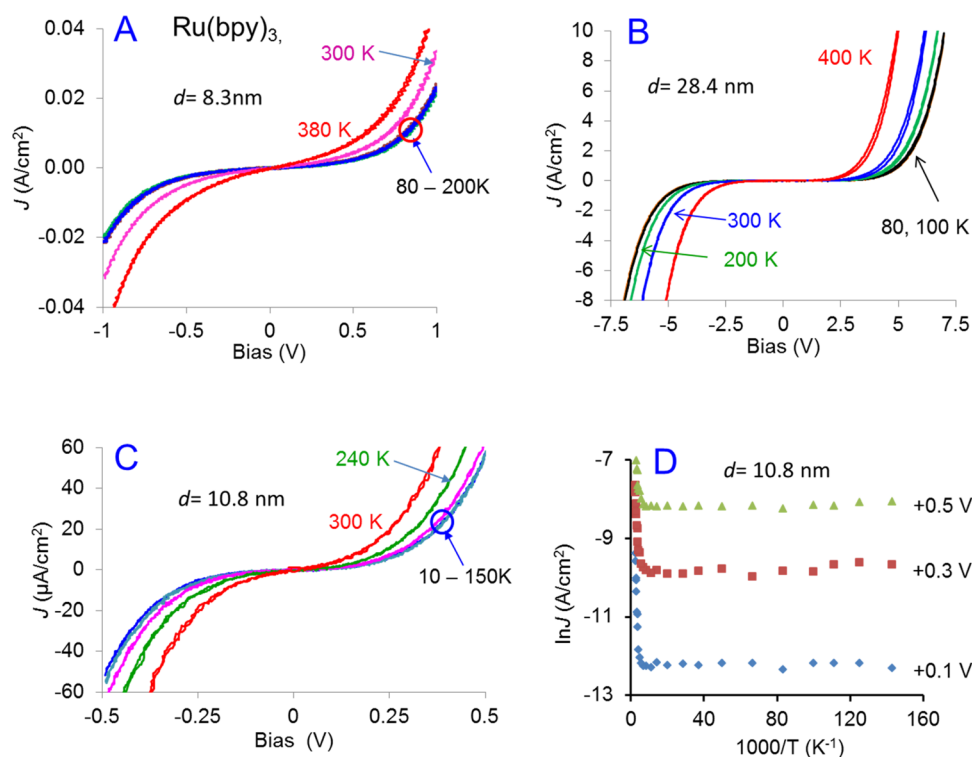


Figure 4. *JV* responses at four temperatures from 80 to 400 K for MJJs with Ru(bpy)₃ with $d = 8.3$ nm (A) and 28.4 nm (B). Panel (C) is from a 10.8 nm MJJ in the range of 10–300 K, as indicated. (D) Arrhenius plot for 10–400 K at three bias voltages.

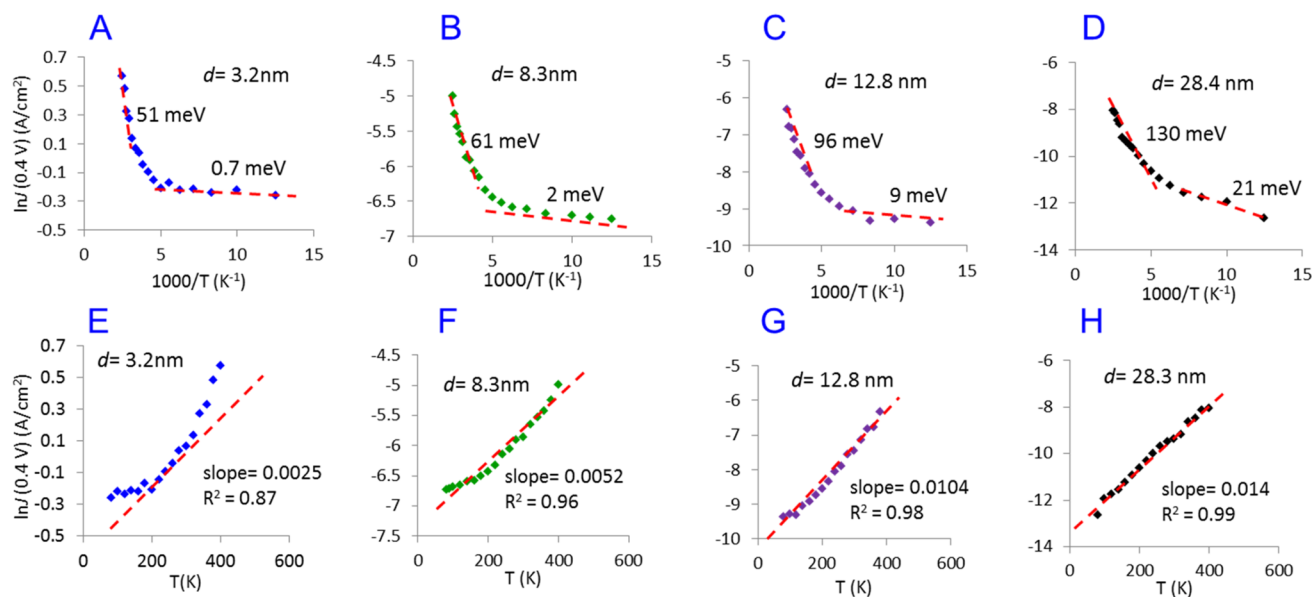


Figure 5. (A–D) Arrhenius plots for the indicated Ru(bpy)₃ thicknesses over the 80–400 K temperature range with apparent activation energies for high and low T regions. (E–H) The same data plotted as $\ln J$ vs T , with slopes and R^2 for linear fits indicated.

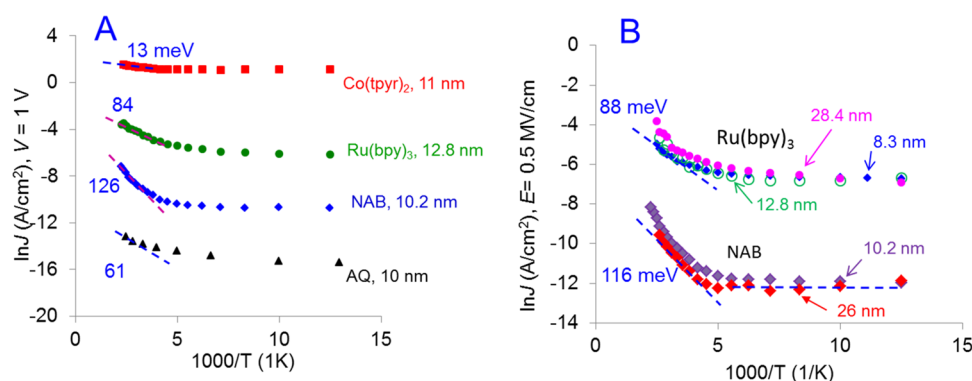
slope occurs for Co(tpy)₂, Ru(bpy)₃, and NAB, but not for AQ. Fourth, $\ln J$ at constant E becomes nearly thickness independent for $d > 10$ nm for all cases except AQ, with $\beta < 0.08$ nm⁻¹ at 1.0 MV/cm.

Temperature dependence is a valuable diagnostic for mechanism, as it indicates possible activation by nuclear motion which might accompany electron transport. *JV* curves ($T = 80$ –400 K) for Ru(bpy)₃ with $d = 8.3$ and 28.4 nm are shown in Figure 4A,B, and additional *JV* curves for $d = 3.2$, 10.8, and 12.8 nm are provided in the SI, Figure S6. For all

thicknesses the current density decreases at lower temperatures, but for $d < 15$ nm the response becomes nearly T independent below 200 K. Figure 4C shows *JV* curves for $d = 10.8$ nm down to 10 K, with the response for 150, 90, and 10 K nearly indistinguishable. As was the case for thinner MJJs,²⁰ the Arrhenius plots of $\ln J$ vs $1/T$ for the 10–400 K range in Figure 4D has two distinct regions, with a near-zero (< 1 meV) slope below 150 K and an activated region from 200–400 K. Arrhenius plots for Ru(bpy)₃ with $d = 3.2$, 8.3, 10.8, and 28.4 nm in the 80–200 K range are shown in Figure 5A–D. At low

Table 2. Arrhenius Slopes of $\text{Co}(\text{tpy})_2$, $\text{Ru}(\text{bpy})_3$, NAB, and AQ MJs for Different Thicknesses at Various Bias in Different T Range

molecule	d (nm)	T (K)	E_a (meV)					
			0.4 V	0.5 V	1 V	1.5 V	2 V	2.5 V
$\text{Ru}(\text{bpy})_3$	3.2	80–200	0.66					
		200–260	14.0					
		260–400	51.4					
	8.3	80–200	1.3	1.0				
		200–260	31.9	27.5				
		260–400	61.6	52.8				
	10.8	10–100			0.07			
		100–200			1.4			
		260–400			84.8			
	12.8	80–200	9.1	4.5	3.0	3.0		1.8
		200–260	57.7	48.1	42.4	38.8		32.8
		260–400	96.4	88.9	84.0	87.4		75.4
28.4	80–200	21.1		21.0	18.9		17.3	
	200–260	70.6		61.2	56.7		53.8	
	260–400	129.7		119.2	112.1		99.7	
$\text{Co}(\text{tpy})_2$	11	80–200		0.3	0.3			
		240–380		19.7	13.8			
NAB	13	80–200		4.6	5.1	5.1		
		240–380		137.2	126.6	116.0		
	26	80–200				0.74	0.49	
		260–400				120.6	106.0	
AQ	10	80–200			10.6	4.5		
		240–400			60.7	92.0		
BTB ^a	10.5	100–200		8	8	8		
		200–300			79			
		22	100–200			43		
		200–300			160			

^aData from ref 16.**Figure 6.** (A) Arrhenius plots for $\text{Co}(\text{tpy})_2$, $\text{Ru}(\text{bpy})_3$, NAB, and AQ MJs with a similar thickness of 10–13 nm and 1 V bias, with apparent activation energies for high T segments as indicated. (B) Arrhenius plots for three thicknesses of $\text{Ru}(\text{bpy})_3$ and two of NAB acquired at a constant electric field of 0.5 MV/cm.

T and $d = 3.2$ nm, the plot exhibits behavior typical of tunneling, with nearly flat T dependence below 200 K ($E_{\text{act}} = 1.6$ meV) and E_{act} of 51 eV for 260–400 K. We concluded previously for NAB devices and $d < 5$ nm that the apparent activation above 200 K is likely due to Fermi function broadening,²⁰ although it may also result from mechanism changes. As the $\text{Ru}(\text{bpy})_3$ thickness increases, the Arrhenius slopes increase to as much as 150 meV near room temperature, but the low T slopes remain less than 25 meV for 80–200 K (summarized in Table 2). As noted previously for thinner MJs of fluorene, AQ, and NAB, Arrhenius plots are curved when plotted over a wide temperature range, but the same data

plotted as $\ln J$ vs T were much closer to linear behavior.⁶ Figure 5E–H shows such plots for the same data as Figure 5A–D, along with the correlation coefficient for a linear fit. The 12.8 and 28.4 nm $\text{Ru}(\text{bpy})_3$ have nearly linear $\ln J$ vs T behavior over the 80–400 K range, with slopes that increase with thickness, whereas $\ln J$ vs T is not linear for $d < 10$ nm.

Arrhenius plots for $\text{Co}(\text{tpy})_2$, $\text{Ru}(\text{bpy})_3$, NAB, and AQ with similar thicknesses of 10–13 nm are compared in Figure 6A for a bias of 1.0 V, with apparent activation energies indicated in the figure and in Table 2. All four molecules have Arrhenius slopes of less than 11 meV below 200 K, but the slopes increase significantly above 200 K. Note that the $\text{Co}(\text{tpy})_2$

case, which is the most conductive of the four molecules compared, also has the weakest T dependence, with Arrhenius slopes (E_{act}) below 20 meV over the 80–380 K range and less than 1 meV below 200 K. Note that Ru(bpy)₃ and NAB have behavior similar to that of BTB (also in Table 2) reported previously, for which E_{act} for $d = 22$ nm decreased from 160 meV at 300 K to less than 1 meV below 100 K.¹⁶

In light of the overlap of JV responses for different thickness at a constant field (Figure 2C,D), the possibility that transport is controlled by the electric field rather than applied bias was tested over a range of temperatures. Not surprisingly, Arrhenius plots at a constant field in Figure S7A are very similar to Figure 6A, with similar apparent activation energies. However, Arrhenius plots for different thicknesses of Ru(bpy)₃ at a constant field (Figure 6B) overlap, despite more than a 2× thickness range. NAB for $d = 10$ and 26 nm shows similar behavior, although with J lower by a factor of ~400. Although the Arrhenius slopes of Figure 5 and Table 2 are both thickness and bias dependent, the situation is different when considered at a constant electric field. As is consistent with Figure 3D, the molecular structure has a strong effect on current density at a given electric field, but for $d > 10$ nm, both transport and temperature dependence are independent of thickness for a given molecule, provided the electric field is constant. As shown in Figure 5H and SI Figures S7B and S8B, both Ru(bpy)₃ and NAB exhibit linear dependence of $\ln J$ vs T above 100 K when $d > 25$ nm.

DISCUSSION

As noted in the Introduction, the main objective of the current paper is understanding how molecular orbital energies affect charge transport when the molecular layer thickness exceeds 5 nm. The Frontier orbital energies for the four molecules studied are provided in Table 3, based on both density

Table 3. HOMO, LUMO, and HOMO–LUMO Gap Energy from DFT and the Energy of the Main UV–vis Absorption Peak of the Molecular Layer for Six Molecules

molecule	DFT HOMO	DFT LUMO	H–L from DFT	H–L from TD DFT	H–L from UV–vis peak
Co(tpy) ₂ (BF ₄) ₃	−5.26	−3.33	1.93	^a	2.50 (1.1 eV ^b)
Ru(bpy) ₃ (PF ₆) ₂	−5.98	−2.65	3.34	2.84	2.68
BTB ^c	−5.29	−1.48	3.81	3.54	3.46
NAB ^c	−6.66	−3.04	3.62	3.61	3.49
fluorene ^c	−5.75	−0.71	5.04	4.75	4.62
AQ ^c	−7.00	−2.77	4.23	5.10	4.84

^aDid not converge. ^bVoltammetry value. ^cFrom ref 21.

functional theory (DFT) of isolated monomers and UV–vis optical absorption of the molecular layer in an intact MJ.²¹ For Co(tpy)₃, the lower energy d–d optical transition is not allowed, so the smaller H–L value of 1.1 eV is included in Table 3. Note that the four molecules cover a range of both the HOMO and LUMO energies but also the H–L gap, and therefore provide a test of how these energies affect charge transport in the respective MJs. Figure 1A,D show major differences in transport efficiency for the four molecules for $d = 10$ –13 nm, with a range of approximately 7 orders of magnitude of current density between AQ and Co(tpy)₂ for $d = 10$ nm and $V = 0.5$ V.

The obvious changes in slope of the attenuation plots in Figures 1C,D and 3C,D are indicators of possible changes in the transport mechanism with layer thickness, which in turn may be affected differently by orbital energies. Ru(bpy)₃ was studied in greatest detail and will be discussed first, followed by comparisons to the other three molecules.

Although the JV curves for Ru(bpy)₃ in Figure 1B are qualitatively similar, the attenuation plots (Figures 1C and S4B) show three distinct linear regions, with β at $V = 0.1$ V equal to 2.4 nm^{−1} for $d < 5$ nm, 0.7 nm^{−1} for $d = 5$ –10 nm, and 0.17 nm^{−1} for $d = 12$ –28.4 nm. The linear dependence of $\ln J$ on $V^{1/2}$ prevailed for the entire thickness range (Figure 2B) and is very similar to the linearity reported previously for AQ, fluorene (FL), NAB, and bis-thienyl benzene (BTB) for $d = 4$ –11 nm.⁶ We also noted previously that $\ln J/E$ vs $E^{1/2}$ is linear for thick BTB devices for $T = 300$ and <10 K.¹⁶ Whatever the origin of the $\ln J$ vs $E^{1/2}$ linearity, it occurred over all three of the regions evident in the β plots, implying that the effect applies to possibly three distinct transport mechanisms. We proposed previously⁶ that barrier lowering in an applied electric field similar to that in Poole–Frenkel conduction can occur in molecular junctions containing AQ, NAB, FL, or BTB, and controls sequential tunneling between localized states in the molecular layer⁶ and/or field-induced ionization.¹⁶ Although Poole–Frenkel conduction fails to explain the observed temperature dependence, the barrier lowering is T independent and tracks $V^{1/2}$ or $E^{1/2}$ according to eq 1, where ϕ is the barrier height, ϕ_0 is the height at zero field, q is the elementary charge, and $\epsilon\epsilon_0$ is the dielectric constant.

$$\phi = \phi_0 - \left(\frac{q}{4\pi\epsilon\epsilon_0} \right)^{1/2} E^{1/2} \quad (1)$$

We proposed that sequential tunneling may be controlled by such a barrier, and the linearity of the current $\ln J$ vs $E^{1/2}$ results indicate that a similar effect may be present in all three β regions evident in Figure 1C.

Consideration of the current–voltage behavior for Ru(bpy)₃ as a function of electric field rather than bias leads to an unexpected overlap of $\ln J$ vs E curves (Figure 2C) as well as near-zero β slopes for $d > 10$ nm (Figure 2D). The β for $d = 2$ –4 nm is similar for either constant V or constant E when $d < 5$ nm, but decreases to <0.06 nm^{−1} at constant E for $d > 10$ nm. Three β regions are not evident in the constant E format, but the slope decreases from ~0.7 nm^{−1} for $V = 0.5$ V to ~0.2 nm^{−1} for $E = 0.5$ MV/cm. It is well-known from Ohm's law and resistivity equations that $J = V\rho/d = E\rho$, where ρ is the resistivity in Ω cm and d the length of the conductor along the conduction axis. Furthermore, conventional semiconductor mobility equations predict field-dependence, i.e., $J = qN\mu E$, where N is the number of carriers and μ is the mobility in cm²/(V s). We are not proposing that conduction in MJs follows the same mechanism as classical resistors or bulk semiconductors, but rather that behavior similar to Ohmic conduction or semiconductor mobility results in J being constant at a given electric field over a range of molecular layer thickness. Stated differently, Ohmic or semiconductor behavior also predicts $\beta = 0$ for constant E , which is close to the observed behavior in Figure 2D, as well as the approximate overlap of JE curves for $d = 10$ –28 nm (Figure 2C). The results clearly support the conclusion that conduction in Ru(bpy)₃ is controlled by E rather than V , at least when $d > 10$ nm. Although Ohmic behavior is expected for several hopping

modes of transport reported in molecular junctions which are sufficiently thick to prevent coherent tunneling,^{8,22,23} the nature of the “hop” and what controls it may vary significantly for different molecular structures and junction designs. In addition, the length of successive hops of carriers may depend strongly on the molecular structure and degree of delocalization.

The device thicknesses for the temperature dependence of the Ru(bpy)₃ MJs (i.e., 3.2, 8.2, 12.8, 28.4 nm) shown in Figures 4 and 5 were chosen to represent the three different β regions of the attenuation plots apparent in Figure 1C. As noted above, the $d = 2\text{--}5$ nm region has temperature dependence consistent with coherent tunneling below 200 K, and weak activation ($E_a < 0.1$ eV) above 200 K. As d increases, the two slopes of the Arrhenius plots become less distinct, and $\ln J$ vs T becomes more linear for $d > 12$ nm. We proposed previously that the $\ln J$ vs T linearity could be a manifestation of sequential tunneling, in this case with a barrier that depends on the electric field.⁶ “Multistep tunneling” was considered for semiconductors in the previous literature, and often results in non-Arrhenius temperature dependence.^{24–27} An obvious consequence of a step-wise mechanism is the necessity for “sites” where carriers temporarily reside during transport. Such sites must involve injection into molecular orbitals, preceded or accompanied by nuclear reorganization. The 12–30 nm thickness range studied here exhibits activated, field-dependent incoherent transport with an unusual $\ln J$ vs T temperature dependence consistent with multistep tunneling. Even for $d = 28$ nm, the molecular layers studied here have not reached the “bulk” behavior of organic semiconductors, in which transport is often mediated by activated redox exchange between sites governed by Marcus kinetics and the reorganization energies of the relevant radical cations and anions. Such bulk transport should have classical Arrhenius behavior over a wide temperature range, with negligible transport below 10 K. Although the linear $\ln J$ vs T dependence may have several origins and may not indicate a unique transport mechanism, proposed transport modes for the NAB and Ru(bpy)₃ studied here must be consistent with linearity when d exceeds ~ 12 nm.

The intermediate $\beta = 0.7$ nm⁻¹ region for $d = 5\text{--}12$ nm of Ru(bpy)₃ has a definite activationless region below 100 K (Figure 4D), and activation above 200 K up to ~ 150 meV for $d = 12.8$ nm. We attributed a similar effect in BTB to field ionization, in which carriers are injected into orbitals by the high applied field, followed by a sequence of steps between adjacent molecules by “intrachain” hopping.¹⁶ As one progresses up the entries of Table 3, the offset between the HOMO and LUMO orbitals and the contact Fermi level (~ -4.8 eV)¹⁹ decreases, such that field ionization or injection becomes more likely. For Ru(bpy)₃, the offsets between the Fermi level and the HOMO or LUMO are approximately equal at ~ 1.3 eV, and we proposed a bipolar injection mechanism which resulted in light emission following reorganization.¹⁸ A recent alternative approach on thinner MJs described how Marcus kinetics can become activationless at high bias, depending on the electronic coupling between molecules and contacts.²⁸ Results on SAM-based large area MJs with a rectifying bilayer structure were consistent with a Marcus inversion mechanism, and transport became activationless for certain molecular structures in the range of 250–330 K, which reverted to Arrhenius linearity when additional aliphatic carbons were inserted in the conduction path.²⁹

When comparing Ru(bpy)₃ to the three other molecules studied, there are some similarities but also pronounced differences. AQ, NAB, and Ru(bpy)₃ have similar current densities for $d = 2\text{--}4$ nm, with β in the 2–3 nm⁻¹ range, whereas Co(tpy)₂ shows comparable J and much lower β value even though there are too few points to reliably determine β below $d = 4$ nm. As noted above and reported previously, the 1–5 nm thickness range for many aromatic molecules is weakly sensitive to structure due to strong coupling between the molecules and the carbon electrodes.^{6,16} Although the Ru(bpy)₃ and Co(tpy)₂ molecules are structurally distinct from the aromatic series studied previously, these differences do not significantly affect transport for the strongly coupled carbon/molecule/carbon MJ structure, when d is less than 3–5 nm. However, once d exceeds 5 nm, major changes in electronic behavior become apparent, with $J(0.5$ V, 8 nm) now covering more than 6 orders of magnitude and β decreasing significantly [e.g., 2.37–0.73 nm⁻¹ for Ru(bpy)₃]. We reported previously¹⁶ that BTB exhibits three β regions, with slopes of 2.9, 1.0, and 0.13 nm⁻¹, quite similar to the Ru(bpy)₃ results of Figure 1C, and we also reported a decreased β for NAB when d exceeded 4 nm.^{6,18} For BTB, a $\beta = 1.0$ nm⁻¹ region was observed for $T = 7\text{--}300$ K, with Arrhenius slopes below 10 meV, compared to the 3–9 meV values observed for Ru(bpy)₃ with $d = 8\text{--}13$ nm and $T = 80\text{--}200$ K (Table 2). Collectively, these results indicate that the second β region ($d = 5\text{--}10$ nm) for Ru(bpy)₃ has similarly weak temperature dependence compared to NAB and BTB, but with widely varying current magnitudes. We also note that all three cases show linearity of $\ln J$ with either $V^{1/2}$ or $E^{1/2}$. Co(tpy)₂ does not exhibit obvious changes in β with thickness, but does share a weak T dependence and $\ln J$ vs $V^{1/2}$ linearity. We previously attributed this behavior to a sequential tunneling mechanism for NAB, BTB, FL, and AQ in the 5–10 nm thickness range, with a field-dependent tunneling barrier, and will consider this possibility further below.⁶

The third region above $d = 12$ nm apparent in Figures 1C and 3C have similar linearity of $\ln J$ vs $V^{1/2}$ to that of Ru(bpy)₃ for all four molecules, and Co(tpy)₂ and NAB also exhibit β near-zero when measured at a constant electric field of 1.0 V/cm (Figure 3D). This region was inaccessible for AQ due to instrumental sensitivity, but a similar plot for BTB based on previous data with a slightly different junction structure¹⁶ showed $\beta = 0.03$ nm⁻¹ at constant E in the format of Figure 3D and $d > 12$ nm (SI Figure S9). To summarize the similarities of the electronic behaviors of Co(tpy)₂, Ru(bpy)₃, NAB, AQ, and BTB for the thickness range of 5–28.4 nm: (1) they all show linearity of $\ln J$ vs $V^{1/2}$, (2) all but AQ show a significant decrease in β when $d > 5$ nm, (3) all but AQ become E -field dependent above ~ 10 nm, and (4) all show a significant decrease in Arrhenius slope to < 50 meV below 200 K and < 10 meV, when $d < 12$ nm. For the 28.3 nm thick Ru(bpy)₃ device (Figure 5H) and NAB (Figure S8), $\ln J$ vs T is linear ($R^2 > 0.99$) over the range of 80–400 K. We now turn to the important question of how the various molecules differ in electronic behavior and the relationship to molecular orbitals and their energies.

Since all devices studied have the same device structure, with covalent bonding to the bottom eC contact and similar physisorbed interactions with the top eC contact, the large differences in current density for all cases above $d = 5$ nm must be controlled by the molecular structure. All molecules studied are aromatic oligomers with no known aliphatic linkages in the

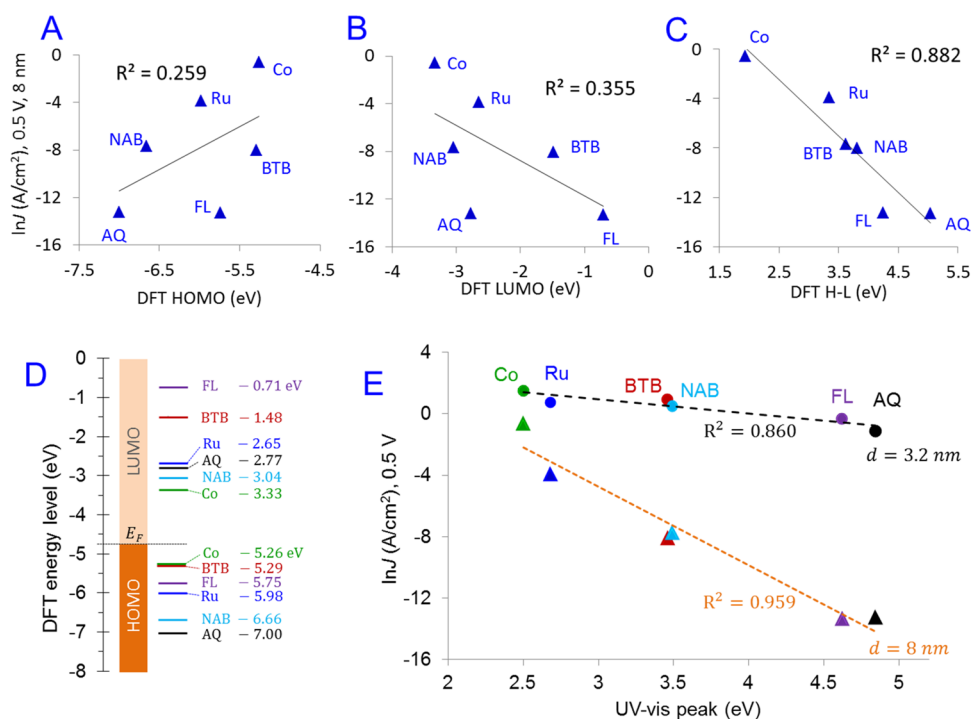


Figure 7. (A) $\ln J$ for $V = 0.5$ V and $d = 8$ nm for $\text{Co}(\text{tpy})_2$, $\text{Ru}(\text{bpy})_3$, NAB, BTB, AQ, FL plotted vs free molecule HOMO energy from DFT [B3LYP/6-31G(d)], (B) the same $\ln J$ plotted vs the DFT LUMO energy of the free molecules, (C) $\ln J$ vs the DFT HOMO–LUMO gap, (D) Relative DFT energy levels from Table 3, (E) $\ln J$ vs the energy of the main UV–vis absorption peak of the molecular layer for $V = 0.5$ V and $d = 3.2$ and 8 nm as indicated. Least squares lines are shown with correlation coefficients.

assumed conduction path, although the degree of conjugation between molecular subunits will likely vary significantly with dihedral angles and other structural differences. We reported previously that the observed $J(V = 0.5$ V) for AQ, BTB, FL, and NAB junctions with $d = 8$ nm correlated with the energy of the UV–vis absorption maximum determined for each molecule directly in a working junction.⁶ Under the postulate that the optical absorption energy is determined by the difference in energies between the molecular HOMO and LUMO levels (the H–L gap), we also proposed that the H–L gap constitutes the barrier for sequential tunneling. A similar analysis of $\text{Co}(\text{tpy})_2$, $\text{Ru}(\text{bpy})_3$, NAB, AQ, FL, and BTB oligomers over a wider range of thicknesses and structures is presented in Figure 7.

As was the case previously⁶ but with the addition of the two metal complexes, the poor correlation between $J(0.5$ V, 8 nm) and either HOMO or LUMO energies is evidence against a transport mechanism based solely on the difference in energy between these orbitals and the electrode Fermi levels, at least for the thick junctions studied (i.e., $d > 5$ nm). The correlation is no better if only donors [i.e., BTB, $\text{Ru}(\text{bpy})_3$, FL, $\text{Co}(\text{tpy})_2$] are considered. For example, $\text{Ru}(\text{bpy})_2$ and fluorene have similar HOMO levels, yet differ by $>10^4$ in current density for the same thickness and bias. Although the correlation of $\ln J$ (0.5 V, $d = 8$ nm) with the DFT H–L gap is better, the measured optical absorption provides the optical H–L gap in the actual MJ. The $\ln J$ vs UV–vis absorption maximum for six molecules and two thicknesses is shown in Figure 7E. As expected from the overlapping attenuation plots for $d < 5$ nm (Figure 1D), $\ln J$ ($d = 3.2$ nm) is weakly dependent on the H–L gap, despite a range from 2.5 to 4.7 eV based on optical absorption. For $d = 8$ nm, the correlation coefficient for $\ln J$ vs UV–vis absorption linearity is 0.959 for a J range of more than

5 orders of magnitude. If the electrochemical H–L value of Co is substituted for the optical value, $R^2 = 0.967$, as shown in Figure S11. Thermal generation of carriers cannot account for the temperature dependence shown in Figure 5, since the 2.68 eV H–L gap for $\text{Ru}(\text{bpy})_3$ predicts the Boltzmann population of much less than 1 carrier/cm² for the entire T range studied. Although the current results do not unequivocally establish that the H–L gap is controlling transport, they do indicate that transport correlates with the magnitude of the H–L gap for the six structures examined.

CONCLUSIONS

The results bear directly on identifying charge transport mechanisms for molecular layers with thicknesses between the limit of ~ 5 nm characteristic of coherent tunneling in aromatic molecular junctions and bulk transport in thick organic films. When $d < 5$ nm and the molecular layers are strongly coupled to the electrodes, molecular structures and energy levels have minor effects on transport, leading to comparable current densities for a wide range of orbital energies. The attenuation plots overlap (Figure 1D) with $\beta = 2\text{--}3$ nm⁻¹ and the temperature dependence is consistent with coherent tunneling. Furthermore, the linear dependence of $\ln J$ on $V^{1/2}$ or $E^{1/2}$ is likely due to the decrease in tunneling barrier in the large applied electric field. For $d > 12$ nm, transport becomes field dependent for at least $\text{Co}(\text{tpy})_2$, $\text{Ru}(\text{bpy})_3$, NAB, and BTB, and exhibits activation above 200 K, similar to that expected for reorganization preceding electron transfer via Marcus theory. However, the near-zero activation energy for NAB and BTB with $d > 20$ nm and $T < 100$ K implies that incoherent tunneling is possible without reorganization preceding electron transport. The intermediate β region when $d = 5\text{--}10$ nm represents a transition from coherent tunneling to bulk

transport, with transport increasing rapidly as the offset between orbital energies and the electrode Fermi level decreases. The correlation of $\ln J$ with the H–L gap in this region may be due to sequential tunneling through barriers related to the H–L energy difference,^{6,21} and/or to injection of charge into orbitals in a redox event.^{18,30} Reorganization may follow injection, but the weak temperature dependence of the $d = 5$ – 10 nm region implies that it follows rather than precedes charge transfer. Whatever the origin of the H–L correlation, it provides one basis for rational design of molecular structures for devices with particular transport properties.

METHODS

The molecular junction fabrication and electronic characterization used previously published procedures^{5,6,16,19} and are described in the Supporting Information for the specific structures in the current paper. Current/voltage curves in figures are averages of at least four molecular junctions of each type and thickness, and were all acquired at a scan rate of 1000 V/s.

ASSOCIATED CONTENT

Supporting Information

The Supporting Information is available free of charge on the ACS Publications website at DOI: 10.1021/acs.jpcc.8b09978.

Fabrication of molecular junctions, electrochemical grafting, thickness measurements by atomic force microscopy “scratching”, additional JV plots for Ru-(bpy)₃, Co(tpy)₂, and NAB junctions, temperature-dependent JV measurements, and UV–vis spectra (PDF)

AUTHOR INFORMATION

Corresponding Authors

*E-mail: lacroix@univ-paris-diderot.fr. Tel.: 00 33 6 18 93 43 28 (J.-C. L.).

*E-mail: richard.mccreery@ualberta.ca. Tel.: 780-641-1760 (R.L.M.).

ORCID

Quyen Van Nguyen: 0000-0003-0120-0971

Amin Morteza Najarian: 0000-0002-0455-0451

Frederic Lafolet: 0000-0001-6313-2308

Jean-Christophe Lacroix: 0000-0002-7024-4452

Richard L. McCreery: 0000-0002-1320-4331

Notes

The authors declare no competing financial interest.

ACKNOWLEDGMENTS

This work was supported by the University of Alberta, the National Research Council of Canada, the Natural Sciences and Engineering Research Council and Alberta Innovates. ANR (France) is gratefully acknowledged for its financial support of this work (ANR-15-CE09 0001-01).

REFERENCES

- (1) Xiang, D.; Wang, X.; Jia, C.; Lee, T.; Guo, X. Molecular-Scale Electronics: From Concept to Function. *Chem. Rev.* **2016**, *116*, 4318.
- (2) Vilan, A.; Aswal, D.; Cahen, D. Large-Area, Ensemble Molecular Electronics: Motivation and Challenges. *Chem. Rev.* **2017**, *117*, 4248.

- (3) Amdursky, N.; Marchak, D.; Sepunaru, L.; Pecht, I.; Sheves, M.; Cahen, D. Electronic Transport Via Proteins. *Adv. Mater.* **2014**, *26*, 7142.

- (4) McCreery, R.; Yan, H.; Bergren, A. J. A Critical Perspective on Molecular Electronic Junctions: There Is Plenty of Room in the Middle. *Phys. Chem. Chem. Phys.* **2013**, *15*, 1065.

- (5) Sayed, S. Y.; Fereiro, J. A.; Yan, H.; McCreery, R. L.; Bergren, A. J. Charge Transport in Molecular Electronic Junctions: Compression of the Molecular Tunnel Barrier in the Strong Coupling Regime. *Proc. Natl. Acad. Sci. U. S. A.* **2012**, *109*, 11498.

- (6) Morteza Najarian, A.; McCreery, R. L. Structure Controlled Long-Range Sequential Tunneling in Carbon-Based Molecular Junctions. *ACS Nano* **2017**, *11*, 3542.

- (7) Choi, S. H.; Risko, C.; Delgado, M. C. R.; Kim, B.; Bredas, J.-L.; Frisbie, C. D. Transition from Tunneling to Hopping Transport in Long, Conjugated Oligo-Imine Wires Connected to Metals. *J. Am. Chem. Soc.* **2010**, *132*, 4358.

- (8) Taherinia, D.; Smith, C. E.; Ghosh, S.; Odoh, S. O.; Balhorn, L.; Gagliardi, L.; Cramer, C. J.; Frisbie, C. D. Charge Transport in 4 Nm Molecular Wires with Interrupted Conjugation: Combined Experimental and Computational Evidence for Thermally Assisted Polaron Tunneling. *ACS Nano* **2016**, *10*, 4372.

- (9) Luo, L.; Balhorn, L.; Vlaisavljevich, B.; Ma, D.; Gagliardi, L.; Frisbie, C. D. Hopping Transport and Rectifying Behavior in Long Donor–Acceptor Molecular Wires. *J. Phys. Chem. C* **2014**, *118*, 26485.

- (10) Kuang, G.; Chen, S.-Z.; Wang, W.; Lin, T.; Chen, K.; Shang, X.; Liu, P. N.; Lin, N. Resonant Charge Transport in Conjugated Molecular Wires Beyond 10 Nm Range. *J. Am. Chem. Soc.* **2016**, *138*, 11140.

- (11) Sedghi, G.; Garcia-Suarez, V. M.; Esdaile, L. J.; Anderson, H. L.; Lambert, C. J.; Martin, S.; Bethell, D.; Higgins, S. J.; Elliott, M.; Bennett, N.; Macdonald, J. E.; Nichols, R. J. Long-Range Electron Tunneling in Oligo-Porphyrin Molecular Wires. *Nat. Nanotechnol.* **2011**, *6*, 517.

- (12) Karipidou, Z.; Branchi, B.; Sarpasan, M.; Knorr, N.; Rodin, V.; Friederich, P.; Neumann, T.; Meded, V.; Rosselli, S.; Nelles, G.; Wenzel, W.; Rampi, M. A.; von Wrochem, F. Ultrarobust Thin-Film Devices from Self-Assembled Metal–Terpyridine Oligomers. *Adv. Mater.* **2016**, *28*, 3473.

- (13) Tuccitto, N.; Ferri, V.; Cavazzini, M.; Quici, S.; Zhavnerko, G.; Licciardello, A.; Rampi, M. A. Highly Conductive 40-Nm-Long Molecular Wires Assembled by Stepwise Incorporation of Metal Centres. *Nat. Mater.* **2009**, *8*, 41.

- (14) Koliwoška, V.; Valášek, M.; Gál, M.; Sokolová, R.; Bulíčková, J.; Pospíšil, L.; Mészáros, G.; Hromadová, M. Single-Molecule Conductance in a Series of Extended Viologen Molecules. *J. Phys. Chem. Lett.* **2013**, *4*, 589.

- (15) Nguyen, Q. V.; Martin, P.; Frath, D.; Della Rocca, M. L.; Lafolet, F.; Bellinck, S.; Lafarge, P.; Lacroix, J.-C. Highly Efficient Long-Range Electron Transport in a Viologen-Based Molecular Junction. *J. Am. Chem. Soc.* **2018**, *140*, 10131.

- (16) Yan, H.; Bergren, A. J.; McCreery, R.; Della Rocca, M. L.; Martin, P.; Lafarge, P.; Lacroix, J. C. Activationless Charge Transport across 4.5 to 22 Nm in Molecular Electronic Junctions. *Proc. Natl. Acad. Sci. U. S. A.* **2013**, *110*, 5326.

- (17) Bayat, A.; Lacroix, J.-C.; McCreery, R. L. Control of Electronic Symmetry and Rectification through Energy Level Variations in Bilayer Molecular Junctions. *J. Am. Chem. Soc.* **2016**, *138*, 12287.

- (18) Tefashe, U. M.; Nguyen, Q. V.; Lafolet, F.; Lacroix, J.-C.; McCreery, R. L. Robust Bipolar Light Emission and Charge Transport in Symmetric Molecular Junctions. *J. Am. Chem. Soc.* **2017**, *139*, 7436.

- (19) Morteza Najarian, A.; Szeto, B.; Tefashe, U. M.; McCreery, R. L. Robust All-Carbon Molecular Junctions on Flexible or Semi-Transparent Substrates Using “Process-Friendly” Fabrication. *ACS Nano* **2016**, *10*, 8918.

- (20) Bergren, A. J.; McCreery, R. L.; Stoyanov, S. R.; Gusarov, S.; Kovalenko, A. Electronic Characteristics and Charge Transport

Mechanisms for Large Area Aromatic Molecular Junctions. *J. Phys. Chem. C* **2010**, *114*, 15806.

(21) Morteza Najarian, A.; Bayat, A.; McCreery, R. L. Orbital Control of Photocurrents in Large Area All-Carbon Molecular Junctions. *J. Am. Chem. Soc.* **2018**, *140*, 1900.

(22) Smith, C. E.; Odoh, S. O.; Ghosh, S.; Gagliardi, L.; Cramer, C. J.; Frisbie, C. D. Length-Dependent Nanotransport and Charge Hopping Bottlenecks in Long Thiophene-Containing Π -Conjugated Molecular Wires. *J. Am. Chem. Soc.* **2015**, *137*, 15732.

(23) Choi, S. H.; Kim, B.; Frisbie, C. D. Electrical Resistance of Long Conjugated Molecular Wires. *Science* **2008**, *320*, 1482.

(24) Roberts, G. G.; Polanco, J. I. Thermally Assisted Tunnelling in Dielectric Films. *Phys. Status Solidi A* **1970**, *1*, 409.

(25) Roberts, G. G.; Apsley, N.; Munn, R. W. Temperature Dependent Electronic Conduction in Semiconductors. *Phys. Rep.* **1980**, *60*, 59.

(26) Riben, A. R.; Feucht, D. L. Electrical Transport in Nge-Pgaas Heterojunctions[†]. *Int. J. Electron.* **1966**, *20*, 583.

(27) Martinuzzi, S.; Mallem, O. Dark-Current Conduction Processes in Cds–Cu₂s Thin-Film Photocells. *Phys. Status Solidi A* **1973**, *16*, 339.

(28) Migliore, A.; Schiff, P.; Nitzan, A. On the Relationship between Molecular State and Single Electron Pictures in Simple Electrochemical Junctions. *Phys. Chem. Chem. Phys.* **2012**, *14*, 13746.

(29) Yuan, L.; Wang, L.; Garrigues, A. R.; Jiang, L.; Annadata, H. V.; Anguera Antonana, M.; Barco, E.; Nijhuis, C. A. Transition from Direct to Inverted Charge Transport Marcus Regions in Molecular Junctions Via Molecular Orbital Gating. *Nat. Nanotechnol.* **2018**, *13*, 322.

(30) de Nijs, B.; Benz, F.; Barrow, S. J.; Sigle, D. O.; Chikkaraddy, R.; Palma, A.; Carnegie, C.; Kamp, M.; Sundararaman, R.; Narang, P.; Scherman, O. A.; Baumberg, J. J. Plasmonic Tunnel Junctions for Single-Molecule Redox Chemistry. *Nat. Commun.* **2017**, *8*, No. 994.